,

Nonlinear electron dynamics in spherical metal clusters

Jérôme Hurst
Institut de Physique et Chimie des Matériaux de Strasbourg, CNRS and University of Strasbourg, 23, rue du Loess – BP 43 – F-67034 Strasbourg, France

Fernando Haas*
Departamento de Física, Universidade Federal do Paraná, 81531-990, Curitiba, Paraná, Brazil

Giovanni Manfredi† and Paul-Antoine Hervieux
Institut de Physique et Chimie des Matériaux de Strasbourg, CNRS and University of Strasbourg, 23, rue du Loess – BP 43 – F-67034 Strasbourg, France
(Dated: December 17, 2013)

The collective electron dynamics in metal clusters is studied using a semiclassical approach based on quantum hydrodynamics. The model incorporates the principal quantum many-body features, such as the Hartree potential and exchange and correlation effects. Through a variational method, the hydrodynamic equations are reduced to a simple set of differential equations, which are used to determine the ground state and the linear response of the cluster. The nonlinear response is explored by means of numerical simulations. We show that, by irradiating the cluster with a chirped laser pulse with slowly varying frequency (autoresonance), it is possible to drive the electron dynamics far into the nonlinear regime, leading to the complete ionization of the cluster on a timescale of the order of 100 fs. The accompanying radiated power spectrum is significantly broad.

PACS numbers: 36.40.Gk, 36.40.Vz, 73.63.-b

I. INTRODUCTION

Metal clusters [1] are mesoscopic systems composed of a relatively small number of metallic atoms, typically between a few tens and several millions. In many respects, metal clusters behave as giant "atoms" where the positive charge is not localized in the nucleus but is distributed more or less uniformly within the cluster. Indeed, their electronic ground state reveals a shell structure with discrete energy levels, akin to those of ordinary atoms. Large metal clusters represent a bridge between molecules and bulk solids. As such, they often exhibit properties belonging to both of these classes of objects and therefore are of great fundamental and practical interest.

Experimentally, it is nowadays possible, by means of ultrafast spectroscopy techniques, to assess the femtosecond dynamics of the electron gas confined in a metal clusters [2–4], so that the theoretical predictions can be directly compared to the experimental measurements. Typical experiments involve perturbing the electron charge and spin with an ultrashort light pulse (the pump), followed by a second weaker pulse (the probe) that acts as a diagnostic tool. By modulating the relative amplitude of the signals, as well as the delay between the pump and the probe, it is possible to measure with great precision the dynamical relaxation of the electron gas.

From the theoretical and computational point of view, metal clusters are generally described using fully quantum treatments based on the density functional theory (DFT), the random phase approximation (RPA) [5, 6], or Hartree-Fock models. The linear response of metal clusters has been the object of intense investigations in the last few decades [7, 8]. A strong dipole resonance is observed near the Mie frequency, which for spherical clusters in the jellium approximation is given by the bulk plasma frequency divided by $\sqrt{3}$. Using more sophisticated approaches, it can be shown that the resonant frequency actually depends on the cluster size.

The nonlinear electron response is much harder to simulate numerically using many-body approaches such as the time-dependent DFT [9]. A possible alternative relies on the use of macroscopic models based on a set of quantum hydrodynamic (QHD) equations [10, 11]. The QHD equations are obtained by taking velocity moments of the Wigner phase-space probability density. Lower-order moments are related to physically relevant quantities such as the particle density, average velocity, and pressure. Hydrodynamic methods were successfully used in the past to model the electron dynamics in molecular systems [12], metal clusters and nanoparticles [13–15], thin metal films [16], quantum plasmas [17, 18] and semiconductors [19].

Even the QHD equations are still relatively hard to

*Electronic address: ferhaas@fisica.ufpr.br
†Electronic address: giovanni.manfredi@ipcms.unistra.fr

solve numerically. In order to achieve a further degree of simplification, we developed a variational approach that expresses the QHD model in the form of a Lagrangian density $\mathcal{L}$ that depends on the relevant hydrodynamic variables, e.g., the density n, the average velocity $\mathbf{u}$, and the potential V. By postulating a reasonable Ansatz for these variables (e.g., a Gaussian profile for the density, as was done in Ref. [15]) it is possible to obtain a set of ordinary differential equations for some macroscopic quantities such as the center of mass and the radial extension of the electron cloud. These equations can then be investigated analytically or solved numerically with very modest computational effort.

In this work, we focus on the collective oscillations of the electron dynamics in metal clusters. This type of oscillations can be excited using a laser pulse. Usually, the wavelength of the laser light (in the visible range, $\lambda \sim 400 - 800$nm) is much longer than the diameter of the cluster ($d \sim 5 - 50$nm), so that the laser excites an electronic dipole mode, corresponding to collective oscillations of the center of mass of the electron population. As the ion mass is thousands of times that of the electrons, it is appropriate – when studying effects occurring on a short timescale (< 100 fs) – to assume that the ions are effectively immobile and that they can be modeled by a uniform positive charge density (jellium approximation).

Using the variational approach, we will study the electron dynamics in a similar way as was done in Ref. [15] for electron-positron plasmas. For the ground state and the linear response regime, our results will be compared to the standard results of metal cluster theory [1, 5–8].

Subsequently, we will investigate the excitation of strongly nonlinear collective electron oscillations. In particular, we will show that a metal cluster can be completely ionized by exciting the electron gas with a chirped laser pulse with slowly varying frequency (autoresonance). Thanks to the autoresonant technique, the instantaneous frequency of the system approaches and stays locked to the varying frequency of the driving field, so that the resonant match is never lost and the amplitude of the oscillations can grow without limits (until, of course, other effects start playing a role). Autoresonant effects were observed in many different physical systems, ranging from atomic physics [20, 21] to fluid dynamics [22], plasmas [23, 24], nonlinear waves [25, 26], planetary systems [27, 28], and quantum oscillators [29–31].

The autoresonant technique is very flexible and efficient, inasmuch as no feedback mechanism is required to match the driving frequency with the oscillator frequency. The only requirement is that the former varies slowly in time. This technique could be used experimentally to induce the rapid and complete ionization of an assembly of metal clusters.

II. QUANTUM HYDRODYNAMIC MODEL

In order to study the electron dynamics in a metal cluster, we make use of a quantum hydrodynamic (QHD) model [10, 11] that governs the evolution of a small number of macroscopic quantities, such as the electron density $n(\mathbf{r}, t)$, mean velocity $\mathbf{u}(\mathbf{r}, t)$, and pressure $P(\mathbf{r}, t)$. In the rest of this work, all quantities are expressed in atomic units, whereby space is normalized to the Bohr radius $a_0 = 4\pi\epsilon_0\hbar^2/(me^2)$, energy to the Hartree energy $E_H = me^4/(4\pi\epsilon_0\hbar)^2$, and time to $t_H = \hbar/E_H$.

The QHD model is based on a set of two hydrodynamic equations

$$\frac{\partial n}{\partial t} + \nabla \cdot (n\mathbf{u}) = 0, \tag{1}$$

$$\frac{\partial \mathbf{u}}{\partial t} + \mathbf{u} \cdot \nabla \mathbf{u} = \nabla V_H - \nabla V_X - \frac{\nabla P}{n} + \frac{1}{2}\nabla\left(\frac{\nabla^2\sqrt{n}}{\sqrt{n}}\right) \tag{2}$$

coupled to Poisson's equation for the Hartree potential V_H:

$$\nabla^2 V_H = 4\pi\,(n - n_i)\,, \tag{3}$$

where $n_i(\mathbf{r})$ is the density of the ion bulk.

Equation (1) is the continuity equation representing conservation of mass, while Eq. (2) is an Euler equation that provides the evolution of the mean velocity under the action of the forces that appear on the right-hand side. The mean-field part of the electron-electron interactions is taken into account by the Hartree potential V_H. The potential V_X represents the exchange interaction:

$$V_X = -\frac{(3\pi^2)^{1/3}}{\pi} n^{1/3} - \frac{4\beta}{3}\frac{(\nabla n)^2}{n^{7/3}} + 2\beta\frac{(\nabla n)^2}{n^{4/3}}, \tag{4}$$

where the first term is the local density approximation (LDA) and the other two terms constitute a gradient correction. The prefactor β is a free parameter that we set equal to $\beta = 0.005$, which is a best-fit frequently used in atomic-structure calculations [32]. For the pressure P we use the standard expression of the Fermi pressure for a zero-temperature electron gas:

$$P = \frac{1}{5}\left(3\pi^2\right)^{2/3} n^{5/3}, \tag{5}$$

which is an acceptable approximation because the Fermi temperature for metals is much larger than ordinary temperatures (e.g., for gold, $T_F = 64200$ K). The last term, often referred to as the von Weizsäcker correction or the Bohm potential, takes into account quantum diffraction effects. The details of the derivation of the QHD model can be found in Ref. [11]. Note that correlation effects have been ignored so far. They can be included in the QHD model in the form of a density-dependent correlation potential $V_C[n(\mathbf{r}, t)]$, which is done in Sec. IV. In practice, the corrections brought by the inclusion of correlation effects are rather minimal.

Variational method.— It can be showed that the hydrodynamic model (1)-(2) can be derived from the following Lagrangian density [15, 19]

$$\mathcal{L} = n\left[\frac{\partial S}{\partial t} + \frac{(\nabla S)^2}{2}\right] + \frac{(\nabla n)^2}{8n} + \frac{3}{10}\left(3\pi^2\right)^{2/3} n^{5/3} - \frac{3}{4\pi}\left(3\pi^2\right)^{1/3} n^{4/3} - \beta\frac{(\nabla n)^2}{n^{4/3}} - \frac{(\nabla V_H)^2}{8\pi} + (n_i - n)\, V_H. \tag{6}$$

This Lagrangian density depends on three scalar fields, namely the density $n(\mathbf{r},t)$, the Hartree potential $V_H(\mathbf{r},t)$, and the phase function $S(\mathbf{r},t)$, which is related to the mean velocity $\mathbf{u}$ by the expression $\mathbf{u} = \nabla S$.

We consider a neutral spherical metal cluster composed of N electrons and N singly-ionized ions, with N typically varying between 10 and 10^6. We adopt a jellium approximation, i.e., we assume that the ions are fixed and form a homogeneous positive charge distribution inside the cluster. Therefore, the ion density can be written as

$$n_i = \begin{cases} n_c, & r \le R, \\ 0, & r > R, \end{cases} \tag{7}$$

where $r = |\mathbf{r}|$ and R is the radius of the cluster, which is related to the Wigner-Seitz radius r_s by the expression: $R = r_s N^{1/3}$. The ions density in the cluster is given by $n_c = N/\left(\frac{4}{3}\pi R^3\right)$.

Our purpose is to derive, using a variational approach, a set of evolution equations for a small number of macroscopic quantities that characterize the electron density profiles [15, 19]. For this, we need a suitable Ansatz for the electron density. To a good approximation, the electron density in a metal cluster is flat and equal to n_c inside the cluster ($r \le R$), while it decreases smoothly to zero near $r = R$ (see Fig. 1). Some electrons are present beyond the nominal cluster radius R, an effect know as *spill-out*. More accurate quantum calculations show that the electron density displays some oscillations (Friedel oscillations), which originate from quantum interference of the wave functions corresponding to different energy levels. These oscillations cannot be recovered by our semi-classical QHD approach.

In order to reproduce qualitatively such a density profile, we assume that the electron density has the following form:

$$n(r,t) = \frac{A}{1 + \exp\left[\left(\frac{s}{\sigma(t)}\right)^3 - \left(\frac{R}{\sigma_0}\right)^3\right]}, \tag{8}$$

where $A = 3N/(4\pi\sigma^3)\left[\ln\left(1+\exp\left(R/\sigma_0\right)^3\right)\right]^{-1}$ is chosen to satisfy the normalization condition $\int n d\mathbf{r} = N$, and s is a displaced radial coordinate defined as $s(t) = \sqrt{x^2 + y^2 + [z - d(t)]^2}$. In the above expression, we introduced two macroscopic dynamical variables, namely:

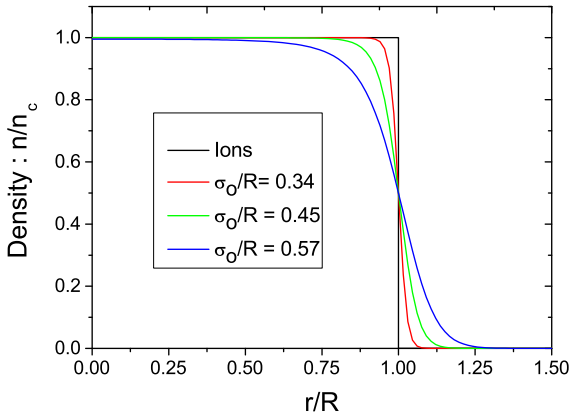

FIG. 1: *Color online.* Schematic view of the ion and electron densities for different values of the spill out parameter σ_0.

(i) the center of mass of the electron gas $d(t)$, which can be displaced along the z axis; and (ii) the thickness of the spill-out effect $\sigma(t)$. At equilibrium, one must have $d = 0$ and $\sigma = \sigma_0$. The value of the spill-out at equilibrium, σ_0, is not predetermined and must be computed self-consistently, as it will be shown later. The electron density issued from Eq. (8) is plotted in Fig. 1, and satisfies the expected properties $\int n d\mathbf{r} = N$ and $\int nz d\mathbf{r}/N = d$.

Of course, such an Ansatz is not exact and may even differ significantly from the electron density obtained, for instance, from DFT calculation [33]. Nevertheless, it is a useful expression, since it will allow us to describe two types of electronic motions: a dipole mode $d(t)$ along the z axis and a breathing mode that corresponds to oscillations of the spill-out thickness through $\sigma(t)$.

We first need to obtain an expression for the two other fields, S and V_H, as a function of the dynamical variables $d(t)$ and $\sigma(t)$. In order to determine $S(\mathbf{r},t)$, or equivalently the mean velocity $\mathbf{u}(\mathbf{r},t)$, we insert Eq. (8) into the continuity equation (1). This yields the exact solution

$$\mathbf{u} = \frac{\dot\sigma}{\sigma}\left(x\widehat{x} + y\widehat{y}\right) + \left[\frac{\dot\sigma}{\sigma}(z-d) + \dot d\right]\widehat{z}, \tag{9}$$

which gives

$$S = \frac{\dot\sigma}{2\sigma}\left[x^2 + y^2 + (z-d)^2\right] + \dot d\,(z-d)\,, \tag{10}$$

where the dot stands for differentiation with respect to time.

In order to obtain the Hartree potential, we rewrite the last two terms in Eq. (6) as

$$-\frac{(\nabla V_H)^2}{8\pi} + (n_i - n)V_H = \frac{(\nabla V_H)^2}{8\pi} - \frac{\nabla\cdot(V_H\nabla V_H)}{4\pi}. \tag{11}$$

The last (divergence) term disappears upon integration over space for reasonable boundary conditions, so that

only the gradient of V_H is required. We decompose the Hartree potential as $V_H = V_i + V_e$, where $V_{i,e}$ are the contributions due to the ions and the electrons respectively, which satisfy the equations: $\nabla^2 V_i = -4\pi n_i$ and $\nabla^2 V_e = 4\pi n$. Assuming spherical symmetry and integrating once in the radial co-ordinate, we find

$$\frac{\partial V_i(r)}{\partial r} = \begin{cases} -\dfrac{N}{R^3} r \ , & r \leq R \\ -\dfrac{N}{r^2} \ , & r > R \end{cases} \tag{12}$$

and

$$s^2 \frac{\partial V_e(s,t)}{\partial s} = \frac{N}{\ln(1+1/a)} \left\{ \frac{s^3}{\sigma^3} - \ln\left[1 + a\exp(s^3/\sigma^3)\right] + \ln(1+a) \right\}, \tag{13}$$

where we introduced the small parameter $a = \exp\left(-R^3/\sigma_0^3\right)$. Note that Eq. (13) is well-behaved both for $s \to 0$ and $s \to \infty$.

Having obtained the expressions for the fields n, S, and ∇V_H – given by Eqs. (8), (10), (12) and (13) – we may proceed to integrate the Lagrangian density (6) with respect to the radial variable in order to obtain the Lagrangian function $L(d,\sigma)$. The only difficulty arises from the cross term $\int (\nabla V_e \cdot \nabla V_i) d\mathbf{r}$, which can only be found in terms of a power series in the variable d/R. Skipping the details, which are given in the Appendix A, we obtain up to order $O(d^5/R^5)$:

$$L = \frac{-1}{N} \int \mathcal{L} d\mathbf{r} = \frac{M(a)\dot{\sigma}^2}{2} - U(\sigma) + \frac{\dot{d}^2}{2} - \frac{\Omega_d^2(\sigma) d^2}{2} + K(\sigma) d^4, \tag{14}$$

where the fictitious mass

$$M(a) = -\frac{\Gamma(5/3)\mathrm{Li}_{5/3}(-1/a)}{\ln(1+1/a)} > 0 \tag{15}$$

is given in terms of a gamma function $\Gamma(5/3) \simeq 0.90$ and a polylogarithm function $\mathrm{Li}_{5/3}$ [39]. The multiplicative factor $-(1/N)$ was introduced in Eq. (14) for convenience of notation. The other terms in Eq. (14) are the pseudo-potential

$$U(\sigma) = \frac{f_B(a)}{\sigma^2} + \frac{N^{2/3} f_F(a)}{\sigma^2} - \frac{N^{1/3} f_X(a)}{\sigma} - \frac{\beta f_{X'}(a)}{N^{1/3}\sigma} + \frac{N f_{ee}(a)}{\sigma} - \frac{N f_{ei}(\sigma)}{R} \tag{16}$$

and the functions

$$\Omega_d^2(\sigma) = \frac{N}{R^3 \ln(1+1/a)} \left\{ \frac{R^3}{\sigma^3} + \ln(1+a) - \ln\left[1 + a\exp(R^3/\sigma^3)\right] \right\}, \tag{17}$$

$$K(\sigma) = \frac{9NRa}{40\ln(1+1/a)\sigma^6} \frac{\exp(R^3/\sigma^3)}{\left[1 + a\exp(R^3/\sigma^3)\right]^2}, \tag{18}$$

which are both positive definite.

The quantities f_B, f_F, f_X, $f_{X'}$, f_{ee} and f_{ei}, which appear in the pseudo-potential (16), are given explicitly in the Appendix A. They are related respectively to the Bohm potential, Fermi pressure, exchange energy (LDA), gradient correction to the exchange energy, electron-electron and electron-ion Hartree interaction terms. All these functions are positive, in accordance with the role played by the Bohm, Fermi and electron-electron terms, which are repulsive, and by the exchange and the electron-ion terms, which are attractive. The quantity $\Omega_d^2(\sigma)$ corresponds to the second order term in the development of the electron-ion interacting energy, whereas $K(\sigma)$ corresponds to the fourth order.

Using the Euler-Lagrange equations

$$\frac{d}{dt}\frac{\partial L}{\partial \dot{\zeta}} - \frac{\partial L}{\partial \zeta} = 0 \ , \tag{19}$$

where $\zeta = \{d, \sigma\}$, we obtain the following coupled equations of motion

$$\ddot{\sigma} = \frac{1}{M(a)} \left\{ -\frac{dU(\sigma)}{d\sigma} + \frac{3Nd^2}{2\sigma^4 \ln(1+1/a)} \frac{1}{1 + a\exp(R^3/\sigma^3)} - \frac{27NRa\exp(R^3/\sigma^3) d^4}{40\ln(1+1/a)\sigma^{10}} \times \frac{\left[1 - a\exp(R^3/\sigma^3)\right] R^3 + 2\left[1 + a\exp(R^3/\sigma^3)\right]\sigma^3}{\left[1 + a\exp(R^3/\sigma^3)\right]^3} \right\}, \tag{20}$$

$$\ddot{d} = -\Omega_d^2(\sigma) d + 4K(\sigma) d^3, \tag{21}$$

which describe respectively the breathing and dipole oscillations.

The approximation made on the Lagrangian (14) (expansion to the fifth order in d/R) has an impact only on the dipole equation (21), which should in principle contain an infinite number of odd terms in the variable d. We kept the lowest order that leads to a nonlinear term in the dipole equation.

In summary, we have reduced the formidable problem of the quantum electron dynamics in a metal cluster (which requires, in principle, a complex DFT or at least mean-field approach) to a simple set of two coupled differential equations. Note that no assumption of linearity was made so far, so that Eqs. (20)-(21) can be used to study the nonlinear response (as long as d is not too large). Various results based on the above equations will be presented in the next Sections.

III. GROUND STATE AND LINEAR RESPONSE

Ground state.— The ground state of the system is obtained by setting the time derivatives equal to zero in

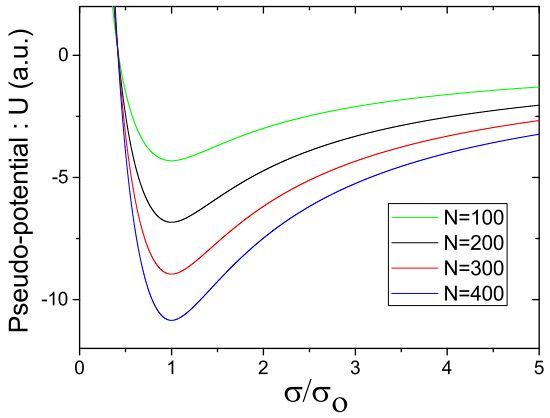

FIG. 2: *Color online.* Plot of the pseudo-potential $U(\sigma)$ given by Eq. (16) as a function of σ, for different cluster sizes. As expected, $U(\sigma)$ has a single minimum located at $\sigma = \sigma_0$.

Eqs. (20)-(21). Equation (21) is satisfied automatically for $d = 0$ (meaning that the center of mass of the ions and the electrons should coincide). Setting $d = 0$ in Eq. (20), the stable equilibria are then the minima of the pseudo-potential $U(\sigma)$, defined by $\sigma = \sigma_0$ such that $U'(\sigma_0) = 0$ and $U''(\sigma_0) > 0$ (see Fig. 2). In the present case the pseudo-potential U depends itself on the equilibrium value σ_0 (through the functions f_B, f_F, etc..., see Appendix A). Therefore, an iterative process should be applied to find σ_0 with a certain precision, starting from a trial value.

Results for gold clusters ($r_s = 3.01$) are given in Table I for different cluster sizes. The ratio of the spill-out thickness σ_0 to the radius of the cluster R decreases with increasing number of particles in the cluster (Fig. 3), in agreement with known results [33].

Linea response.— Having determined the ground state of the system (i.e., the value of σ_0) we can proceed to study the linear response of the electron gas. There are two linear modes, corresponding to oscillations of $\sigma(t)$ (breathing mode) and oscillations of $d(t)$ (dipole mode).

We first consider the breathing frequency, denoted by Ω_b. Setting $d = 0$ in Eq. (20) and expanding $U(\sigma)$ around σ_0 up to first order, we obtain $M(a)\ddot{\sigma} = U''(\sigma_0)(\sigma - \sigma_0)$. The linear breathing frequency is therefore:

$$\Omega_b = \left[\frac{1}{M(a)}\frac{d^2U}{d\sigma^2}(\sigma_0)\right]^{1/2}. \qquad (22)$$

Next, we consider the dipole mode. Assuming that $\sigma = \sigma_0$ and $d \ll 1$, Eq. (21) becomes: $\ddot{d} + \Omega_d^2(\sigma_0)d = 0$. From Eq. (17) the linear dipole frequency is then

$$\Omega_d = \sqrt{\frac{N}{R^3\ln(1+1/a)}\left[\frac{R^3}{\sigma_0^3} + \ln\left(\frac{1+a}{2}\right)\right]}. \qquad (23)$$

N	R	σ_0	Ω_d	Ω_b
50	11.09	6.24	0.1793	0.2988
100	13.97	7.21	0.1821	0.3059
150	15.99	7.86	0.1835	0.3093
200	17.60	8.36	0.1843	0.3114
250	18.96	8.77	0.1848	0.3129
300	20.15	9.12	0.1852	0.3141
350	21.21	9.43	0.1856	0.3150
400	22.18	9.70	0.1859	0.3158
450	23.07	9.95	0.1861	0.3164

TABLE I: Ground-state and linear-response parameters for gold clusters of different sizes. All quantities are expressed in atomic units.

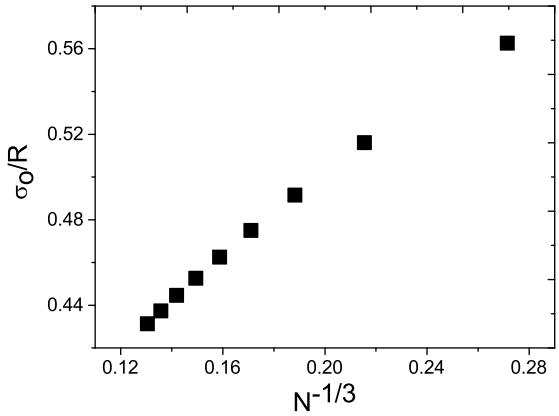

FIG. 3: Ratio of the spill-out parameter σ_0 to the cluster radius R versus $N^{-1/3}$, for gold clusters. The values are taken from Table I. The spill-out thickness becomes less important with increasing N.

The results for the breathing and dipole frequencies are summarized in Table I.

For large clusters, the dipole frequency should be equal to the Mie frequency [1, 34]

$$\omega_{Mie} = \frac{\omega_p}{\sqrt{3}} = \sqrt{\frac{4\pi n_c}{3}}, \qquad (24)$$

where $\omega_p = \sqrt{4\pi n_c}$ is the plasmon frequency in atomic units. Indeed, taking the limit $R/\sigma_0 \to \infty$ in Eq. (23) and making use of the expressions $a = \exp(-R^3/\sigma_0^3) \to 0$ and $n_c = N/(4\pi R^3/3)$, one finds exactly the Mie frequency defined above.

In the general case, the dipole frequency depends on number of particles in the cluster. It has been shown that this dependence is of the following form [5]:

$$\Omega_d(N) = \omega_{Mie}\left(1 - \frac{k}{N^{1/3}}\right), \qquad (25)$$

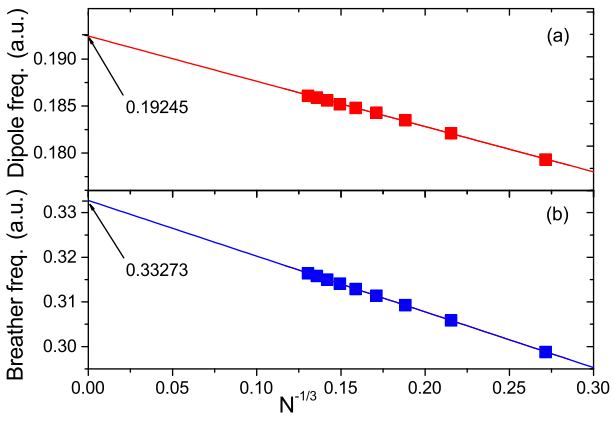

FIG. 4: *Color online.* Linear dipole (red squares, top panel) and breathing (blue squares, bottom panel) frequencies versus $N^{-1/3}$, taken from Table I. The straight lines are linear fits. The extrapolation to $N \to \infty$ yields the respective bulk frequencies. Note that their ratio is very close to $\sqrt{3}$.

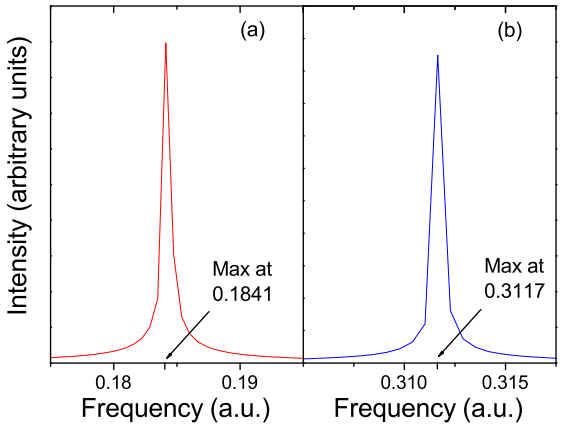

FIG. 5: *Color online.* Simulated frequency spectrum for the dipole mode (left panel) and the breathing mode (right panel) for gold clusters with $N = 200$.

where $k > 0$. Our model reproduces very well this $N^{-1/3}$ law, as can be seen from Fig. 4a, which displays the dipole frequency as a function of N, using the data of Table I. The extrapolation at $N \to \infty$ gives the Mie frequency in the bulk.

Interestingly, a similar behavior is also found for the breathing frequency Ω_b, as shown in Fig. 4b. Although the N dependence is the same, the bulk breathing frequency is given by the plasmon frequency rather than the Mie frequency, so that we have

$$\Omega_b(N) = \omega_p \left(1 - \frac{k'}{N^{1/3}}\right), \tag{26}$$

where $k' > 0$ and $\omega_p = \sqrt{3}\omega_{Mie}$. This can be understood by noting that the dipole oscillations are a surface mode, whereas the breathing oscillations are a volume mode. This behavior was already observed in DFT calculations of Al and Na metal clusters [6].

Finally, we show the results of some numerical simulations of Eqs. (20)-(21) in the linear regime. We start from a configuration close to equilibrium (ground state with $d = 0$ and $\sigma = \sigma_0$), then we perturb it slightly and observe the subsequent oscillations of $d(t)$ and $\sigma(t)$. The frequency spectra of these oscillations are plotted in Fig. 5 for $N = 200$. The observed maxima are located very close to the theoretical dipole and breathing frequencies listed in Table I, thus validating the numerical simulations.

IV. CORRELATION EFFECTS

So far, our model included exchange effects but no other type of correlations. In the framework of DFT, correlations can be introduced through an appropriate functional of the electron density. Here, we use the functional proposed by Brey et al. [35], which yields the following correlation potential

$$V_C = -\gamma \ln\left[1 + \alpha n^{1/3}\right], \tag{27}$$

with $\gamma = 0.03349$ and $\alpha = 18.376$. With this potential, the Euler equation becomes

$$\begin{aligned} \frac{\partial \mathbf{u}}{\partial t} + \mathbf{u}\nabla\mathbf{u} &= \nabla V_H - \nabla V_X - \nabla V_C - \frac{1}{mn}\nabla P \\ &+ \frac{\hbar^2}{2m^2}\nabla\left[\frac{\nabla^2\sqrt{n}}{\sqrt{n}}\right]. \end{aligned} \tag{28}$$

In order to include this correlation potential, the following term needs to be added to the Lagrangian density

$$\begin{aligned} \mathcal{L}_C &= -\frac{\gamma}{6\alpha^3}\Big[-6\alpha n^{1/3} + 3\alpha^2 n^{2/3} - 2\alpha^3 n \\ &+6\left(1+\alpha^3 n\right)\ln\left(1+\alpha n^{1/3}\right)\Big]. \end{aligned} \tag{29}$$

This yields a new term in the integrated Lagrangian of the system:

$$\begin{aligned} L_C &= -\frac{1}{N}\int \mathcal{L}_C \, d\mathbf{r} \\ &= \frac{2\pi\gamma}{3\alpha^3 N}\Big[-6\alpha\bar{A}^{1/3}I_1\sigma^2 + 3\alpha^2\bar{A}^{2/3}I_2\sigma \\ &-2\alpha^3 N + 6I_3(\sigma)\sigma^3\Big], \end{aligned} \tag{30}$$

where

$$\bar{A} = A\sigma^3 = \frac{3N}{4\pi}\left[\ln\left(1+\exp\left(\frac{R}{\sigma_0}\right)^3\right)\right]^{-1},$$
$$I_1 = \int_0^\infty \frac{X^2}{[1+a\exp(X^3)]^{1/3}}dX,$$
$$I_2 = \int_0^\infty \frac{X^2}{[1+a\exp(X^3)]^{2/3}}dX,$$
$$I_3(\sigma) = \int_0^\infty X^2\left[1+\frac{B(X)^3}{\sigma^3}\right]\ln\left[1+\frac{B(X)}{\sigma}\right]dX,$$

and

$$B(X) = \frac{\alpha\bar{A}^{1/3}}{[1+a\exp(X^3)]^{1/3}}.$$

The resulting corrections can be incorporated in the pseudo-potential function $U(\sigma)$. The new terms are as follows

$$U_C(\sigma) = f_c\sigma^2 - f_{c'}\sigma - f_{c''}I_3(\sigma)\sigma^3, \qquad (31)$$

where

$$f_c = \frac{4\pi\gamma}{\alpha^2 N}\bar{A}^{1/3}I_1,$$
$$f_{c'} = \frac{2\pi\gamma}{\alpha N}\bar{A}^{2/3}I_2,$$
$$f_{c''} = \frac{4\pi\gamma}{\alpha^3 N}.$$

Notice that the correlation effects only affect the equation for σ, but not the dipole. The properties of the ground state will also be modified, in particular the equilibrium value of the spill-out thickness σ_0. Nevertheless, these changes remain quite small, for instance σ_0 decreases by only 3%. The results for the ground state and the linear response with correlations are summarized in Table II.

In Fig. 6 we compare the linear dipole and breathing frequencies with and without correlations. Both frequencies are slightly larger when correlations are included, but the difference becomes smaller with increasing cluster size, as it should. For $N \to \infty$ both frequencies converge to their bulk values, respectively ω_{Mie} and ω_p. Correlations may become important for very small systems ($N < 50$), but in that case our QHD model is itself questionable. Finally, the corrections of the pseudo-potential are also quite small, so that we do not expect a significant change in the nonlinear dynamics (see next Section).

V. NONLINEAR RESPONSE AND AUTORESONANT EXCITATION

We now turn our attention to the excitation of the electron and positron dynamics by means of electromagnetic

N	R	σ_0	Ω_d	Ω_b
50	11.09	6.07	0.1803	0.3026
100	13.97	7.0	0.1830	0.3089
150	15.99	7.61	0.1843	0.3118
200	17.60	8.09	0.1850	0.3138
250	18.96	8.48	0.1855	0.3154
300	20.15	8.81	0.1859	0.3162
350	21.21	9.1	0.1862	0.3170
400	22.18	9.37	0.1864	0.3175
450	23.07	9.6	0.1866	0.3182

TABLE II: Ground-state and linear-response parameters for gold clusters of different sizes, including correlations. All quantities are expressed in atomic units.

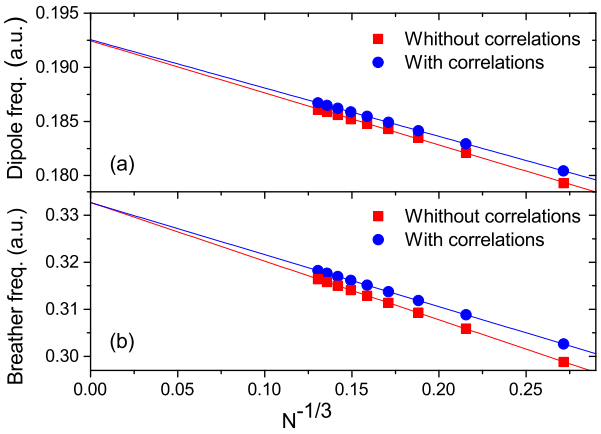

FIG. 6: *Color online.* Linear dipole (a) and breathing (b) frequencies for gold clusters as a function of $N^{-1/3}$. Blue circles and red squares represent respectively the results with and without correlations. The straight lines are linear fits. The data are those of Tables I and II.

waves (laser pulses). First, it should be noted that the relevant linear frequencies computed in the preceding section are of the order of a few electron-volts. For instance, for $N = 200$, $\Omega_d = 0.1841$ a.u. $= 5$ eV. These frequencies fall within the visible or near ultraviolet (UV) spectrum, which is encouraging since visible and near-UV lasers are commonly employed in ultrafast optics experiments. For such lasers, the wavelength is several hundred nanometers long, i.e., much larger than the size of a typical metal cluster (see Table I). This means that the laser pulse can only couple to the dipole mode.

We assume that the electron gas in the cluster is excited via an oscillating electric field directed along the z axis

$$\mathbf{E} = E_z(t)\mathbf{e}_z = E_0\cos(\omega t)\,\mathbf{e}_z, \qquad (32)$$

where ω is the frequency of the laser and E_0 is the amplitude of the electric field.

The interaction energy between the laser and the electron gas is equal to $\int nV_{las}d\mathbf{r}$, where $V_{las} = -zE_z$. The new Lagrangian is obtained by adding this interaction term to the previous Lagrangian

$$L' = L - \frac{1}{N}\int(-nzE_z)dz = L + E_z d, \qquad (33)$$

where L is given in Eq. (14). This correction only changes the equation for d, which becomes

$$\ddot{d} = -\Omega_d^2(\sigma)d + 4K(\sigma)d^3 - E_z(t). \qquad (34)$$

Numerical simulations of the dipole and the breather motions are shown in Fig. 7. We choose the laser frequency equal to the dipole frequency ,i.e., $\omega = \Omega_d$, so that the excitation is resonant. As expected, the dipole oscillations grow rapidly, but then decrease after some time. This is because the effective dipole force [right-hand side of Eq. (34)] is not harmonic and the resonant frequency actually depends on the amplitude of the oscillations. Therefore, when the amplitude increases, the laser frequency will no longer match the instantaneous dipole frequency: the resonant condition is lost and the amplitude of the oscillations $d(t)$ stops growing. We also note that the breathing frequency Ω_b is excited nonlinearly (Fig. 7a), with some delay with respect to the dipole mode.

The above limitation can be overcome by resorting to *autoresonant* excitation [36]. Basically, autoresonance occurs when a classical nonlinear oscillator is externally excited by an oscillating field with slowly varying frequency. In our notation

$$E_z(t) = E_0 \cos\left[\Omega_d(t-t_0) + \frac{1}{2}\alpha(t-t_0)^2\right], \qquad (35)$$

where E_0 is the excitation amplitude. The time-dependent frequency of such excitation is equal to

$$\omega(t) = \Omega_d + \alpha\,(t-t_0)\,. \qquad (36)$$

where t_0 is the time when the instantaneous frequency of the laser is equal to the linear frequency of the dipole mode, and α is the rate of variation of the laser frequency. It can be shown that, for $|\alpha| \ll \Omega_d^2$ and E_0 above a certain threshold, the instantaneous oscillator frequency becomes "locked" to the instantaneous excitation frequency, so that the resonance condition is always satisfied. In that case, the amplitude of the oscillations grows indefinitely and without saturation, until of course some other effect kicks in. It was previously shown [36] that the threshold behaves as $E_0^{\rm th} \sim |\alpha|^{3/4}$, implying that the amplitude can be arbitrarily small, provided that the external frequency varies slowly enough. As mentioned in the Introduction, autoresonant excitation has been been fruitfully applied to a variety of nonlinear systems, ranging from condensed-matter to astrophysics.

In Fig. 8, we display the results of an autoresonant excitation of the electron gas, for two values of the laser

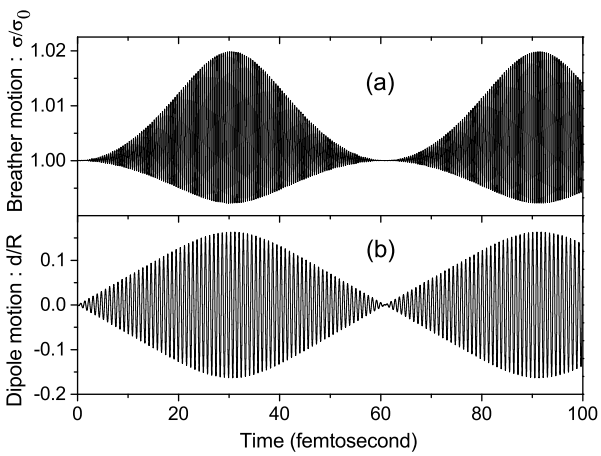

FIG. 7: Nonlinear dynamics of the electron gas in a gold cluster with $N = 200$, excited by a laser field of intensity $E_0 = 6 \times 10^{10}\ W/cm^2$ and constant frequency equal to the dipole frequency, $\omega = \Omega_d$. The form of the laser excitation is given by Eq. (32). Top panel (a): breathing mode; Bottom panel (b): dipole mode.

amplitude E_0 that are either below or above the autoresonant threshold. When $E_0 = 4.5 \times 10^{10}\mathrm{W/cm^2}$ (below threshold, Fig. 8a), the dipole oscillations grow initially and then saturate at a rather low level ($d \approx 0.15R$). For this case, Fig. 8c shows the instantaneous laser frequency and the dipole frequency of the electron gas, which was determined numerically using a Hilbert transform technique [37]. The two frequencies stay close together initially, but then diverge, showing that the autoresonant excitation did not work in this case.

In contrast, when $E_0 = 5.7 \times 10^{10}\mathrm{W/cm^2}$ (above threshold), the amplitude of the dipole oscillations increases virtually without limits, reaching 80% of the size of the cluster (Fig. 8b). Indeed, the laser and the electron gas frequencies are locked to each other during the entire duration of the simulation (Fig. 8d), indicating that the system stays in resonance all the time. This is clearly the hallmark of the autoresonant excitation. We stress that the value $d \approx 0.8R$ means in practice that all the electrons have been ejected from the cluster, which therefore has been completely ionized. This ionization occurs on a very short time scale, of the order of a few hundred femtoseconds.

It should be noted that for large values of d our model is no longer valid. Indeed, since we expanded the Lagrangian to a certain order in d/R, the force acting on the dipole in Eq. (21) becomes repulsive for d exceeding a certain critical value d_{cr} (which depends on σ), whereas in reality it should always be attractive. A mathematical analysis of the equations of motion shows that this critical value reaches its minimum for $\sigma \approx \sigma_0$ (i.e., near equilibrium), where $d_{cr} \simeq 0.65R$. Even with this limitation, our simulations constitute a clear proof of principle that the electron gas can be very strongly excited and the

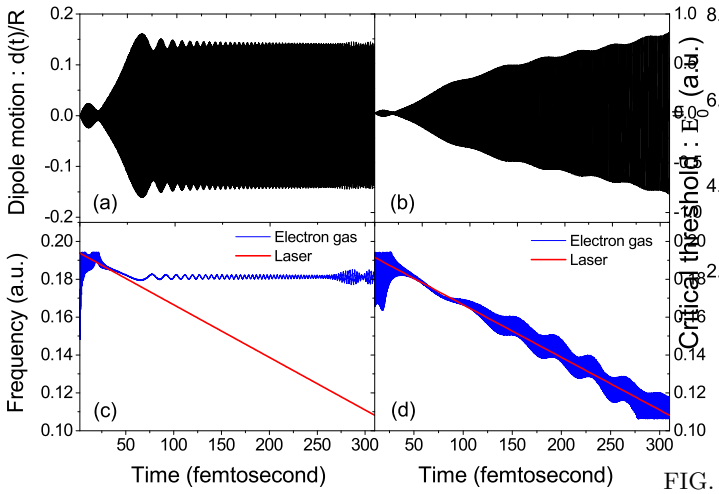

FIG. 8: *Color online.* Autoresonant excitation of a gold cluster with $N = 200$. We set the parameters $\alpha = 6.67 \times 10^{-6}$ a.u. and $t_0 = 36$ fs and use two values of the electric field amplitude, namely $E_0 = 4.5 \times 10^{10}\mathrm{W/cm^2}$ [left panels, (a) and (c)] and $E_0 = 5.4 \times 10^{10}\mathrm{W/cm^2}$ [right panels, (b) and (d)]. The top panels show the time evolution of the dipole $d(t)$, whereas the bottom panels display the laser frequency (red straight line) and the instantaneous dipole frequency of the electron gas (blue curve).

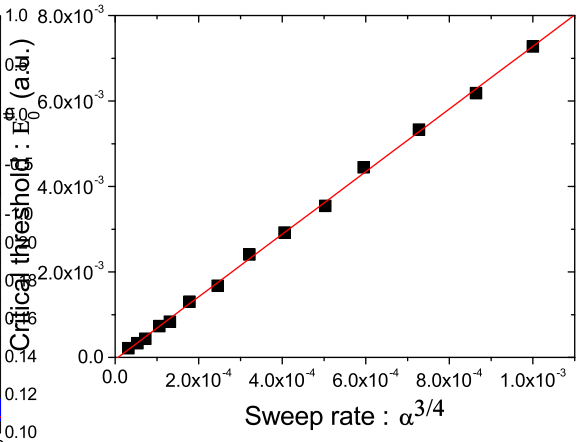

FIG. 9: *Color online.* Critical electric field amplitude (atomic units) for a gold cluster with $N = 200$ as a function of the frequency sweep rate $\alpha^{3/4}$. The theoretical law (red straight line) is well recovered.

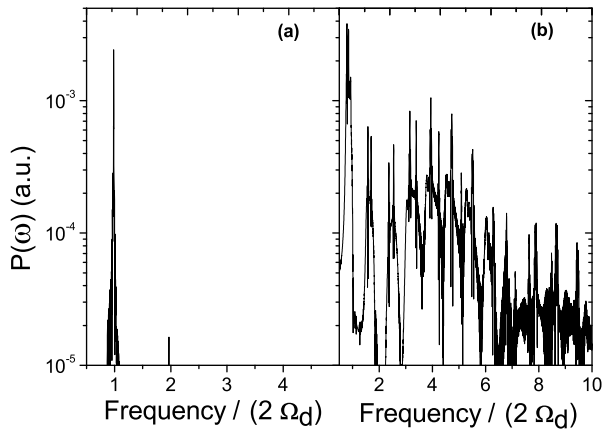

FIG. 10: Frequency spectrum of the total power radiated by the electron gas in a gold cluster with $N = 200$, for two cases: below the autoresonance threshold (a) and above the threshold (b). These two cases correspond to the excitations described in Fig. 8a and b.

cluster completely ionized using an autoresonant ionization.

In Fig. 9, we show the threshold electric field as a function of the frequency sweep rate α. As expected, the threshold field varies as $\alpha^{3/4}$, in agreement with the theory [36] and with the numerical results obtained for a variety of other nonlinear oscillators. This is a further confirmation that we are indeed observing the autoresonant mechanism at work.

It is also interesting to study the total power radiated by the electron gas, for cases above and below the critical threshold at which autoresonance occurs. In order to simplify the problem, we suppose that we are far from the system, so that the electron gas can be viewed as an electric dipole of charge $-Ne$ and displacement $d(t)$ oscillating along the z axis. In this case we can apply the Larmor's formula [38] for the total radiated power:

$$P(t) = \frac{e^2}{6\pi\epsilon_0 c^3}|\ddot{d}(t)|^2. \qquad (37)$$

It is expected that the total power spectrum $P(\omega)$ will be localized around the linear dipole frequency in the below-threshold case (for which the oscillations around the equilibrium are small). In contrast, the spectrum should be rich in higher order harmonics in the above-threshold regime, for which the electron gas explores the nonlinear part of the confining potential.

This behavior was indeed observed in the frequency spectrum of the radiated power, which is plotted in Fig. 8 for two cases. Below threshold (Fig. 8a), as expected, the signal is concentrated around $2\Omega_d$ [the factor two comes from the square of the dipole acceleration in Eq. (37)]. Above threshold (Fig. 8b), several higher-order harmonics are clearly observed.

Such difference in the observed spectrum could in principle be used as an experimental signature to assess the effectiveness of the autoresonant excitation.

VI. CONCLUSION

In this paper, we proposed a simple model for the electron response in a metal cluster using a set of quantum hydrodynamic (QHD) equations. Despite its apparent simplicity, the model contains virtually all relevant electronic effects: (i) the mean-field Hartree potential; (ii) exchange effects (both LDA and gradient corrections); (iii) correlation effects (through a suitable functional); (iv) quantum statistical effects (through the degeneracy or Fermi pressure); and (v) quantum diffraction effects (via the Bohm potential). The ions were represented by a motionless profile of positive charge (jellium model).

The QHD equations can be expressed through a Lagrangian density, which in turn – by assuming a certain Ansatz on the electron density – can be used to derive a simple Lagrangian function that depends only on two parameters: the center of mass of the electron gas $d(t)$ and the thickness of the spill-out effect $\sigma(t)$. The study of the collective electron motion was thus reduced to a system of two coupled differential equations, which can easily be integrated numerically.

The model was validated against known results for the ground state and the linear response, with good qualitative agreement.

One of the advantages of the present approach is that it is not restricted to the linear regime and can deal with the nonlinear dynamics, albeit in a simplified way. As an example of a nonlinear effect, we investigated the electron response to a laser excitation with slowly varying frequency (autoresonant driving). It has been known for a long time that the autoresonance mechanism can be used to excite large-amplitude nonlinear oscillations. Here, we show that this technique can be applied to the electron dynamics in metal clusters.

Indeed, we observe that it is possible to strongly drive the electron gas away from equilibrium and consequently completely ionize the cluster on a timescale of the order of 100 fs. As the ionization is very fast, we can expect that the ions have not yet had time to move, so that the jellium approximation should be valid. The nonlinear electron motion results in a radiated power spectrum that is considerable broad and may be used as an experimental signature of the autoresonant ionization.

Acknowledgments. Labex NIE ?

APPENDIX A: DERIVATION OF THE LAGRANGIAN

The starting point is the Lagrangian density (6), which we can be rewritten, using Eq. (11), as

$$\begin{aligned}\mathcal{L} = & \, n\left[\frac{\partial S}{\partial t}+\frac{(\nabla S)^2}{2}\right]+\frac{(\nabla n)^2}{8n}+\frac{3}{10}\left(3\pi^2\right)^{2/3}n^{5/3} \\ & -\frac{3}{4\pi}\left(3\pi^2\right)^{1/3}n^{4/3}-\beta\frac{(\nabla n)^2}{n^{4/3}} \\ & +\frac{(\nabla V_H)^2}{8\pi}-\frac{\nabla\cdot(V_H\nabla V_H)}{4\pi}.\end{aligned} \tag{A1}$$

The Lagrangian is obtained by integrating the above Lagrangian density over space

$$\begin{aligned}L \;=\; & \frac{-1}{N}\int\mathcal{L}d\mathbf{r}, \\ =\; & -\underbrace{\frac{1}{N}\Big[\int n\frac{\partial S}{\partial t}d\mathbf{r}}_{1}+\underbrace{\frac{1}{2}\int n\left(\nabla S\right)^2 d\mathbf{r}}_{2}+\underbrace{\frac{1}{8}\int\frac{(\nabla n)^2}{n}d\mathbf{r}}_{3} \\ & +\underbrace{\frac{3}{10}\left(3\pi^2\right)^{2/3}\int n^{5/3}d\mathbf{r}}_{4}-\underbrace{\frac{3}{4\pi}\left(3\pi^2\right)^{1/3}\int n^{4/3}d\mathbf{r}}_{5} \\ & -\underbrace{\beta\int\frac{(\nabla n)^2}{n^{4/3}}d\mathbf{r}}_{6}+\underbrace{\frac{1}{8\pi}\int(\nabla V_H)^2 d\mathbf{r}}_{7} \\ & -\frac{1}{4\pi}\int\nabla\cdot(V_H\nabla V_H)d\mathbf{r}\Big].\end{aligned} \tag{A2}$$

The last integral is a surface term which is equal to zero if the Hartree electric field vanishes at infinity.

The first step is to express the quantities $\partial S/\partial t$, $(\nabla S)^2$ and $(\nabla n)^2$ as functions of the dynamical variables $d(t)$, $\sigma(t)$ and of the shifted radial coordinate s. The fields n and S are defined respectively by Eqs. (8) and (10). We obtain

$$\begin{aligned}\frac{\partial S}{\partial t} &= \frac{\ddot{\sigma}\sigma-\dot{\sigma}^2}{2\sigma^2}s^2-\frac{\dot{\sigma}}{\sigma}\dot{d}\,(z-d)+\ddot{d}\,(z-d)-\dot{d}^2, \\ (\nabla S)^2 &= \left[\frac{\dot{\sigma}}{\sigma}\right]^2 s^2+2\frac{\dot{\sigma}}{\sigma}\,(z-d)\,\dot{d}+\dot{d}^2, \\ (\nabla n)^2 &= \frac{9a^2s^4}{A^2\sigma^6}\exp\left[\frac{2s^3}{\sigma^3}\right]n^4.\end{aligned}$$

Now, we are in a position to compute the integrals in the Lagrangian (A2). We evaluate each term separately:

1.

$$\begin{aligned}\int n\frac{\partial S}{\partial t}d\mathbf{r} &= \left[\frac{\ddot{\sigma}}{2\sigma}-\frac{\dot{\sigma}^2}{2\sigma^2}\right]\int ns^2d\mathbf{r}+\left[\ddot{d}-\frac{\dot{\sigma}}{\sigma}\dot{d}\right]\\ &\times\int n\left(z-d\right)d\mathbf{r}-\dot{d}^2\int nd\mathbf{r},\\ &= \left[\frac{\ddot{\sigma}}{2\sigma}-\frac{\dot{\sigma}^2}{2\sigma^2}\right]\int ns^2d\mathbf{r}-N\dot{d}^2. \qquad \text{(A3)}\end{aligned}$$

We used the symmetry properties of the electron density to obtain the above expression. We further compute

$$\begin{aligned}\int ns^2d\mathbf{r} &= A\int\frac{s^2}{1+a\exp\left(s^3/\sigma^3\right)}d\mathbf{r},\\ &= 4\pi A\int_0^\infty\frac{X^4}{1+a\exp\left(X^3/\sigma^3\right)}dX,\\ &= N\sigma^2M(a), \qquad \text{(A4)}\end{aligned}$$

where $M(a)$ is definesd as

$$M(a)=-\frac{\Gamma(5/3)\mathrm{Li}_{5/3}(-1/\mathrm{a})}{\ln(1+1/a)}.$$

Li is a polylogarithm function defined by

$$\mathrm{Li}_n(-1/a)=-\frac{1}{\Gamma(n)}\int_0^\infty\frac{X^{n-1}}{1+a\exp\left(X\right)}dX,$$

with $Xe(n)>0$, Im(a) = 0 and $1/a>-1$. Now we can inject Eq. (A4) into Eq. (A3) to obtain

$$\begin{aligned}\int n\frac{\partial S}{\partial t}d\mathbf{r} &= \frac{N}{2}M(a)\left(\ddot{\sigma}\sigma-\dot{\sigma}^2\right)-N\dot{d}^2,\\ &= \frac{N}{2}M(a)\left[\frac{d}{dt}\left(\sigma\dot{\sigma}\right)-2\dot{\sigma}^2\right]-N\dot{d}^2,\\ &= -NM(a)\dot{\sigma}^2-N\dot{d}^2, \qquad \text{(A5)}\end{aligned}$$

where we suppressed the total time derivative as it does not modify the equations of motion.

2.

$$\begin{aligned}\frac{1}{2}\int n\left(\nabla S\right)^2d\mathbf{r} &= \frac{1}{2}\left[\frac{\dot{\sigma}}{\sigma}\right]^2\int ns^2d\mathbf{r}+\frac{\dot{\sigma}}{\sigma}\dot{d}\\ &\times\int\left(z-d\right)nd\mathbf{r}+\frac{\dot{d}^2}{2}\int nd\mathbf{r},\\ &= \frac{N}{2}M(a)\dot{\sigma}^2+\frac{N}{2}\dot{d}^2. \qquad \text{(A6)}\end{aligned}$$

3.

$$\begin{aligned}\frac{1}{8}\int\frac{\left(\nabla n\right)^2}{n}d\mathbf{r} &= \frac{9\pi a^2A}{2\sigma^6}\int_0^\infty\frac{X^6\exp\left(2X^3/\sigma^3\right)}{\left[1+a\exp\left(X^3/\sigma^3\right)\right]^3}dX,\\ &= \frac{Nf_B(a)}{\sigma^2}, \qquad \text{(A7)}\end{aligned}$$

where f_B is defined as

$$f_B(a)=\frac{27a^2}{8\ln(1+1/a)}\int_0^\infty\frac{X^6\exp\left(2X^3\right)}{\left[1+a\exp\left(X^3\right)\right]^3}dX. \qquad \text{(A8)}$$

4.

$$\begin{aligned}\frac{3\left(3\pi^2\right)^{2/3}}{10}\int n^{5/3}d\mathbf{r} &= \frac{6\pi\left(3\pi^2\right)^{2/3}}{5}A^{5/3}\\ &\times\int_0^\infty\frac{X^2}{\left[1+a\exp\left(X^3/\sigma^3\right)\right]^{5/3}}dX,\\ &= \frac{N^{5/3}f_F(a)}{\sigma^2}, \qquad \text{(A9)}\end{aligned}$$

where f_F is defined as

$$\begin{aligned}f_F(a) &= \frac{6}{5}\left(3\pi\right)^{2/3}\left[\frac{3}{4\ln(1+1/a)}\right]^{5/3}\sigma^3\\ &\times\int_0^\infty\frac{X^2}{\left[1+a\exp\left(X^3\right)\right]^{5/3}}dX. \qquad \text{(A10)}\end{aligned}$$

5.

$$\begin{aligned}\frac{3\left(3\pi^2\right)^{1/3}}{4\pi}\int n^{4/3}d\mathbf{r} &= \left(81\pi^2\right)^{1/3}A^{4/3}\\ &\times\int_0^\infty\frac{X^2}{\left[1+a\exp\left(X^3/\sigma^3\right)\right]^{4/3}}dX,\\ &= \frac{N^{4/3}f_X(a)}{\sigma}, \qquad \text{(A11)}\end{aligned}$$

where f_X is defined as

$$\begin{aligned}f_X(a) &= \left[\frac{9}{4\sqrt{\pi}\ln(1+1/a)}\right]^{4/3}\\ &\times\int_0^\infty\frac{X^2}{\left[1+a\exp\left(X^3\right)\right]^{4/3}}dX. \qquad \text{(A12)}\end{aligned}$$

6.

$$\begin{aligned}\beta\int\frac{\left(\nabla n\right)^2}{n^{4/3}}d\mathbf{r} &= \frac{36\pi a^2A^{2/3}\beta}{\sigma^6}\\ &\times\int_0^\infty\frac{X^6\exp\left(2X^3/\sigma^3\right)}{\left[1+a\exp\left(X^3/\sigma^3\right)\right]^{8/3}}dX,\\ &= \frac{\beta N^{2/3}}{\sigma}f_{X'}(a), \qquad \text{(A13)}\end{aligned}$$

where $f_{X'}(a)$ is defined as

$$\begin{aligned}f_{X'}(a) &= \left(\frac{4\pi}{3}\right)^{1/3}\frac{27a^2}{\left[\ln(1+1/a)\right]^{2/3}}\\ &\times\int_0^\infty\frac{X^6\exp\left(2X^3\right)}{\left[1+a\exp\left(X^3\right)\right]^{8/3}}dX. \qquad \text{(A14)}\end{aligned}$$

7.

$$\begin{aligned}\frac{1}{8\pi}\int(\nabla V_H)^2d\mathbf{r} &= \frac{1}{8\pi}\Bigg[\int(\nabla V_i)^2d\mathbf{r}+\int(\nabla V_e)^2d\mathbf{r}\\ &+2\int\nabla V_i\cdot\nabla V_ed\mathbf{r}\Bigg]. \qquad \text{(A15)}\end{aligned}$$

The first integral in Eq. (A15) does not contribute to the equations of motion because it does not depend on the dynamical variables d or σ. Let us evaluate the other two integrals separately:

$$\int (\nabla V_e)^2 d\mathbf{r} = \int \left[\frac{\partial V_e}{\partial s}\right]^2 d\mathbf{r} = \frac{8\pi N}{\sigma} f_{ee}(a), \qquad \text{(A16)}$$

where $f_{ee}(a)$ is defined as

$$f_{ee}(a) = \frac{1}{2\left[\ln(1+1/a)\right]^2} \int \frac{dX}{X^2} \Big\{ X^3 + \ln(1+a) - \ln\left[1 + a\exp(X^3)\right] \Big\}. \qquad \text{(A17)}$$

Let us call $I(d)$ the third integral in Eq. (A15):

$$\begin{aligned} I(d) &\equiv \int \nabla V_e \cdot \nabla V_i \qquad \text{(A18)} \\ &= \int \frac{\partial V_i}{\partial r}\frac{\partial V_e}{\partial s}\frac{1}{sr}(r^2 - zd) d\mathbf{r} \\ &= \frac{2\pi N}{\ln(1+1/a)} \int \frac{\partial V_i}{\partial r}\frac{r^2 \sin\theta}{s^3}(r - d\cos\theta) \\ &\times \left\{ \frac{s^3}{\sigma^3} - \ln\left[1 + a\exp(s^3/\sigma^3)\right] + \ln(1+a) \right\} dr d\theta, \end{aligned}$$

where we used the expressions (12) and (13), and the angle θ is defined so that $z = r\cos\theta$. We cannot simplify the integral I because it does not possess spherical symmetry. The only way to proceed is to develop the variable $s = \sqrt{x^2 + y^2 + (z-d)^2}$ as a power series of d:

$$s = r - d\cos\theta + \frac{d^2 \sin^2\theta}{2r} + O(d^3).$$

We find that I can be written in terms of a power series of d

$$I = \frac{4\pi N^2 f_{ei}(\sigma)}{R} - 2\pi N \Omega_d^2(\sigma) d^2 + 4\pi N K(\sigma) d^4 + \cdots, \qquad \text{(A19)}$$

where $f_{ei}(\sigma)$, $\Omega_d^2(\sigma)$ and $K(\sigma)$ are given by

$$\begin{aligned} f_{ei}(\sigma) &= \frac{1}{\ln(1+1/a)} \Big\{ \frac{\sigma^2}{R^2} \int_0^{R/\sigma} X\Big[X^3 + \ln(1+a) \\ &- \ln\left(1 + a\exp\left(X^3\right)\right)\Big] dX + \frac{R}{\sigma}\int_{R/\sigma}^{\infty} \frac{dX}{X^2}\Big[X^3 \\ &+ \ln(1+a) - \ln\left(1 + a\exp\left(X^3\right)\right)\Big] \Big\}, \qquad \text{(A20)} \\ \Omega_d^2(\sigma) &= \frac{N}{R^3 \ln(1+1/a)} \Big\{ \frac{R^3}{\sigma^3} + \ln(1+1/a) \\ &- \ln\left[1 + a\exp(R^3/\sigma^3)\right] \Big\}, \qquad \text{(A21)} \\ K(\sigma) &= \frac{9NRa}{40\ln(1+1/a)\sigma^6} \frac{\exp(R^3/\sigma^3)}{\left[1 + a\exp(R^3/\sigma^3)\right]^2}. \qquad \text{(A22)} \end{aligned}$$

The odd powers of d disappears, as expected, because the problem is symmetric with respect to the (x, y) plane, so that the equations should be unchanged if we change d with $-d$.

Injecting Eqs. (A5), (A6), (A7), (A9), (A11), (A13), (A16) and (A19) into Eq. (A2), we obtain the Lagrangian of the system, Eq. (14), with the pseudo-potential defined in Eq. (16).

[1] U. Kreibig and M. Vollmer, *Optical proprieties of metal clusters*, Springer series in material science **25** (1995).
[2] J.-Y. Bigot, V. Halté, J.-C. Merle, and A. Daunois, Chem. Phys. **251**, 181 (2000).
[3] C. Voisin at al., Phys. Rev. Lett. **85**, 2200 (2000).
[4] M. Nisoli et al., Phys. Rev. Lett. **78**, 3575 (1997).
[5] C. Bréchignac et al., Phys. Rev. Lett. **70**, 2036 (1993).
[6] J. G. Aguilar et al., Int. J. Quantum. Chem. **61**, 613 (1997).
[7] W. Ekardt, Phys. Rev. B **31**, 6360 (1985).
[8] C. Guet and W. R. Johnson, Phys. Rev. B **45**, 11283 (1992).
[9] F. Calvayrac, P.-G. Reinhard, E. Suraud, and C. Ullrich, Phys. Rep. **337**, 493 (2000).
[10] F. Haas, *Quantum plasmas an hydrodynamic approach*, Springer, (2011)
[11] G. Manfredi and F. Haas, Phys. Rev. B **64**, 075316 (2001).
[12] M. Brewczyk et al., Phys. Rev. Lett. **78**, 191 (1997).
[13] A. Banerjee, M. K. Harbola, J. Chem. Phys. **113**, 5614 (2000)
[14] A. Domps, P.-G. Reinhard, and E. Suraud, Phys. Rev. Lett. **81**, 5524 (1998).
[15] G. Manfredi, P. A. Hervieux, and F. Haas, New J.Phys. **64**, 075316 (2012)
[16] N. Crouseilles, P.-A. Hervieux, and G. Manfredi,, Phys. Rev. B **78**, 155412 (2008)
[17] B. Eliasson and P. K. Shulka, Phys. Rev. Lett. **96**, 245001 (2006).
[18] B. Eliasson and P. K. Shulka, Phys.-Usp. **53**, 51 (2010).
[19] F. Haas, G. Manfredi, P. K. Shukla, and P.-A. Hervieux, Phys. Rev. B **80**, 073301 (2009).
[20] B. Meerson and L. Friedland, Phys. Rev. A **41**, 5233 (1990).
[21] W. K. Liu, B. Wu and J. M. Yuan, Phys. Rev. Lett. **75**, 1292 (1995).
[22] L. Friedland, Phys. Rev. E **59**, 4106-4111 (1999).
[23] J. Fajans, E. Gilson and L. Friedland, Phys. Rev. Lett. **82**, 4444 (1999).
[24] J. Fajans, E. Gilson and L. Friedland, Phys. Plasmas **6**,

4497 (1999).
[25] I. Aranson, B. Meerson and T. Tajima, Phys. Rev. A **45**, 7500 (1992).
[26] L. Friedland and A.G. Shagalov, Phys. Rev. Lett **81**, 4357 (1998).
[27] R. Malhotra, Sci. Am. **281** (9), 56-63 (1999).
[28] L. Friedland, Astrophys. J. **547** (9), L75 (2001).
[29] I. Barth et al., Phys. Rev. A **84**, 013837 (2011).
[30] K. W. Murch et al., Nature Phys. **7**, 105-8 (2011).
[31] G. Manfredi and P. A. Hervieux, Appl. Phys. Lett. **91**, 061108 (2007).
[32] A. D. Becke, Phys. Rev. A **38**, 6 (1988).
[33] G. Weick, PhD thesis, University of Strasbourg (2006).
[34] G. Mie, Annalen der Physik **330**, 337 (1908)
[35] L. Brey et al., Phys. Rev. B **42**, 2 (1990).
[36] J. Fajans and L. Friedland, Am. J. Phys. **69**, 1096 (2001).
[37] J. C. Goswami and A. E. Hoefel, Signal processing **84**, 1423-1427 (2004).
[38] J. D. Jackson, *Classical electrodynamics* (Wiley, New York, 1998).
[39] The polylogarithm function is defined as $\mathrm{Li}_p(-1/a) = -[1/\Gamma(p)]\int_0^\infty dX\, X^{p-1}/(a\, e^X + 1)$, where $\mathrm{Re}(p) > 0$, $\mathrm{Im}(a) = 0$, and $1/a > -1$.